

MDPI

Article

# A Comparative Study of Geometric Phase Change- and Sideband Peak Count-Based Techniques for Monitoring Damage Growth and Material Nonlinearity

Guangdong Zhang <sup>1,2</sup>, Tribikram Kundu <sup>1,2,3,4,\*</sup>, Pierre A. Deymier <sup>1,4</sup> and Keith Runge <sup>1,4</sup>

- New Frontiers of Sound Science and Technology Center, University of Arizona, Tucson, AZ 85721, USA; guangdongzhang@arizona.edu (G.Z.); deymier@arizona.edu (P.A.D.); krunge@arizona.edu (K.R.)
- Department of Aerospace and Mechanical Engineering, University of Arizona, Tucson, AZ 85721, USA
- Department of Civil and Architectural Engineering and Mechanics, University of Arizona, Tucson, AZ 85721, USA
- Department of Materials Science and Engineering, University of Arizona, Tucson, AZ 85721, USA
- \* Correspondence: tkundu@arizona.edu

**Abstract:** This work presents numerical modeling-based investigations for detecting and monitoring damage growth and material nonlinearity in plate structures using topological acoustic (TA) and sideband peak count (SPC)-based sensing techniques. The nonlinear ultrasonic SPC-based technique (SPC-index or SPC-I) has shown its effectiveness in monitoring damage growth affecting various engineering materials. However, the new acoustic parameter, "geometric phase change (GPC)" and GPC-index (or GPC-I), derived from the TA sensing technique adopted for monitoring damage growth or material nonlinearity has not been reported yet. The damage growth modeling is carried out by the peri-ultrasound technique to simulate nonlinear interactions between elastic waves and damages (cracks). For damage growth with a purely linear response and for the nonlinearity arising from only the nonlinear stress-strain relationship of the material, the numerical analysis is conducted by the finite element method (FEM) in the Abaqus/CAE 2021 software. In both numerical modeling scenarios, the SPC- and GPC-based techniques are adopted to capture and compare those responses. The computed results show that, from a purely linear scattering response in FEM modeling, the GPC-I can effectively detect the existence of damage but cannot monitor damage growth since the linear scattering differences are small when crack thickness increases. The SPC-I does not show any change when a nonlinear response is not generated. However, the nonlinear response from the damage growth can be efficiently modeled by the nonlocal peri-ultrasound technique. Both the GPC-I and SPC-I techniques can clearly show the damage evolution process if the frequencies are properly chosen. This investigation also shows that the GPC-I indicator has the capability to distinguish nonlinear materials from linear materials while the SPC-I is found to be more effective in distinguishing between different types of nonlinear materials. This work can reveal the mechanism of GPC-I for capturing linear and nonlinear responses, and thus can provide guidance in structural health monitoring (SHM).

**Keywords:** topological acoustic sensing; geometric phase change-index (GPC-I); sideband peak count-index (SPC-I); damage monitoring; material nonlinearity; numerical modeling; structural health monitoring



Citation: Zhang, G.; Kundu, T.; Deymier, P.A.; Runge, K. A Comparative Study of Geometric Phase Change- and Sideband Peak Count-Based Techniques for Monitoring Damage Growth and Material Nonlinearity. *Sensors* 2024, 24, 6552. https://doi.org/10.3390/ s24206552

Academic Editor: Victor Giurgiutiu

Received: 22 August 2024 Revised: 4 October 2024 Accepted: 8 October 2024 Published: 11 October 2024



Copyright: © 2024 by the authors. Licensee MDPI, Basel, Switzerland. This article is an open access article distributed under the terms and conditions of the Creative Commons Attribution (CC BY) license (https://creativecommons.org/licenses/by/4.0/).

## 1. Introduction

Ultrasonic nondestructive testing and evaluation (UNDT&E)-based techniques are widely used in engineering structural health monitoring (SHM) to ensure structural safety [1,2]. Nonlinear ultrasonic (NLU) techniques, due to their high sensitivity, are receiving increasing attention over conventional linear acoustic techniques [3–5]. Robust techniques with high sensitivity are desirable for the development of reliable SHM techniques.

Sensors **2024**, 24, 6552 2 of 17

In general, monitoring damage or material evolution using ultrasonic waves relies on linear or nonlinear changes in the waves' main characteristics such as velocity, amplitude, resonance frequency and dynamic phase [6]. For instance, at the early stages of acoustics research, linear parameters like the wave velocity, attenuation and dynamic phase changes were commonly used to detect damage features such as material evolution, porosity of additive manufacturing parts and cracks in plate structures [7–10]. In recent decades, some classic NLU techniques, such as higher harmonics generation (HHG) [11-13] and nonlinear wave modulation spectroscopy (NWMS) or frequency modulation (FM) [14,15] have been used to detect changes in material states. In nonlinear resonance techniques, such as nonlinear impact resonance acoustic spectroscopy or NIRAS, resonance frequency shifts and attenuation variations with increasing amplitudes of excitation are recorded and analyzed [16,17]. Recently, another nonlinear technique called a sideband peak count-index (or SPC-I), which focuses on changes in multiple sideband peak amplitudes, has been proposed [18-25]. A correlation between the amplitude levels of sideband peaks and the degree of nonlinear response has been established [26]. It can be concluded that most currently available NLU techniques are focused on variations in nonlinear amplitude and frequency and can be referred to as magnitude-based or frequency feature-based methods. In spite of the high sensitivity of NLU techniques, limitations and restrictions still exist in terms of their practical implementation.

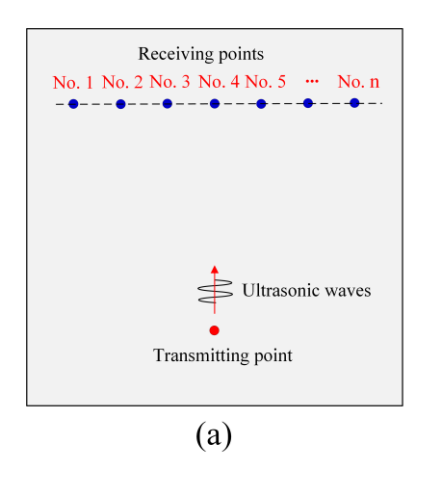
An emerging method called topological acoustic (TA) sensing has recently been introduced to sense defects and environmental and structural changes [6,27–31]. This method utilizes a geometric phase change (GPC) that quantifies the variation in the geometric phase of an acoustic field represented as a state vector in Hilbert space. The states of the acoustic field in the unperturbed (damage-free) and perturbed (damaged) states are mapped as multidimensional vectors in the Hilbert space and compared. By exploiting sharp topological features spanned by the acoustic field's multidimensional state vector, the geometric phase sensing modality can achieve higher sensitivity than magnitude- or frequency-based sensing approaches. This approach is not limited to linear wave fields but can also include nonlinear contributions to the wave field and their associated state vectors.

With the TA sensing technique, changes in complex environments such as forests [27] or the state of permafrost in the arctic [28] have been monitored using seismic waves. This method has been further extended to monitor perturbations in the form of (1) a mass defects located on an array of coupled acoustic waveguides [6], (2) mass defects in a nonlinear granular metamaterial [29] and (3) a small subwavelength object on a flat surface submerged in water [30]. These investigations reported in the literature have introduced the capability of GPC to sense defects by analyzing linear scattering. Such sensitivity with GPC is useful in damage detection. Zhang et al. [31] adopted the GPC technique to monitor damage growth in heterogeneous structures with different topographies using nonlocal peri-ultrasound modeling. They found that GPC is superior to the amplitude-based SPC technique for monitoring damage growth in heterogeneous structures. In peri-ultrasound modeling, both linear and nonlinear scattering can be generated by cracks. Separate investigations of linear and nonlinear responses are needed to arrive at a clear understanding of the mechanism of GPC and its capability of sensing and monitoring damage. Investigations of monitoring material nonlinearity using GPC are also very few.

In this work, in light of the above discussion, a TA sensing technique using GPC is investigated numerically in terms of detecting and monitoring damage and material nonlinearity in plate structures. The GPC-index (GPC-I) is used to detect and monitor perturbations (such as defects) and material evolution using the TA sensing technique. The numerical modeling is carried out by nonlocal peri-ultrasound modeling of damage growth that produces both linear and nonlinear responses. The finite element method (FEM) in the Abaqus/CAE 2021 software is used for damage growth modeling that produces pure linear responses. The comparison of these two numerical methods can thus provide a comprehensive understanding of the effectiveness of the GPC technique for detecting and monitoring damage growth in structures using its linear and nonlinear responses. The

linear responses. The comparison of these two numerical methods can thus provide a comprehensive understanding of the effectiveness of the GPC technique for detecting and monitoring damage growth in structures using its linear and nonlinear responses. The material nonlinearity is modeled in FEM by considering different stress—strain relationships prescribed by the Abaqus/CAE 2021 software. The effect of different constitutive material relationships prescribed by the Abaqus/CAE 2021 software. The effect of different constitutive material relationships on the GPC present uses and prescribed by the Abaqus/CAE 2021 software. The effect of different constitutive material relationships on the GPC unique spectrums and prescribed as on tributions of this paper area.

- (1) Therefore, the pixeposequie feature feature feature feature again alarmage but it is part with the page resitivity;
- (13) The offects of linear and non-linear insparses and the inches violation of the control of t
- (2) The editions with the ar and nonlinear responses on the behavior of GPC-I are investigated
- (3) iA demparison between the available SPC-I technique and the proposed GPC-I technique
- (3) Aigun paristav belv benna elavaitab GPC-lucch taquettucthin parpade nonlinear responses, approcess and eliture an epinanida gura no de la company de la
- (4) The effects of matrices mediane arity SPINAR Splinad GRSC-I are compared;
- (45) The unfolder standing of george PCid phase Plange in applications is
- (5) Altuited mental understanding of geometric phase change in practical applications is clarified.
- 2. Methodology and Theory
- 2. Methodology and Theory and methodology of the proposed TA sensing techniques are problement, the concept and methodology of the proposed TA sensing techniques are problement, the concept and methodology the top crappes (TPC septima techniques are problement that the concept the control of the control o



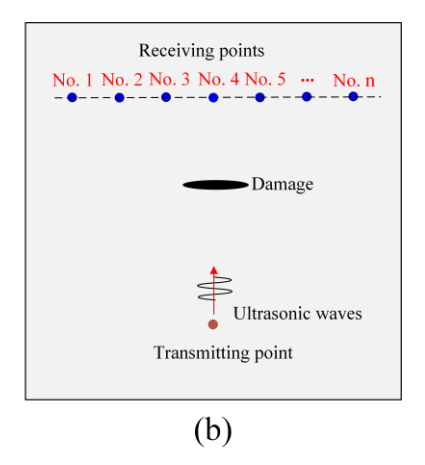


Figure 1. Schematic diagram showings the creference taket and pertitude deate to for ATA ensinging; (a) alabang of deep plate (e deference state) e (b) b) alang of plate (pertitude deate).

Frorthe-reference-state (intractipate-without any damage) at each receiving location (total 11-) locations), shown in Figure 1-2, the displacement of Secretary damage) at each receiving location (total 11-) locations), shown in Figure 1-2, the displacement of Secretary damage are recorded as a time reference that the state in the reference of the state of the secretary damage. The secretary damage is a normalized state vector in an dimensional complex Hilbert space. The n basis vectors of that subspace correspond to locations in the physical space. This normalized state vector can be written as [30]

$$C = \frac{1}{\sqrt{C_1^2 + C_2^2 + C_3^2 + \dots C_n^2}} \begin{pmatrix} C_1 e^{i\phi_1} \\ C_2 e^{i\phi_2} \\ C_3 e^{i\phi_3} \\ \dots \\ C_n e^{i\phi_n} \end{pmatrix}$$
(1)

Sensors **2024**, 24, 6552 4 of 17

In Equation (1),  $C_k$  and  $\phi_k$  (k = 1, 2, 3, ..., n) are the magnitude and spatial phase at each receiving point. The components of this multi-dimensional state vector are the complex amplitudes of the field at every location in the discretized space of the n detectors. When damage is introduced, as shown in Figure 1b, the perturbation in the physical space scatters the acoustic waves and modifies the spatial distribution of the acoustic field. Perturbations such as damage then change the normalized complex amplitude of the acoustic field to

$$C' = \frac{1}{\sqrt{C_1'^2 + C_2'^2 + C_3'^2 + \dots C_n'^2}} \begin{pmatrix} C_1' e^{i\phi_1'} \\ C_2' e^{i\phi_2'} \\ C_3' e^{i\phi_3'} \\ \dots \\ C_n' e^{i\phi_n'} \end{pmatrix}$$
(2)

At a single given frequency f, the angle between the vector representation of the acoustic field along the n locations in the damage-free and damaged systems corresponds to a change in the geometric phase of the acoustic wave. This angle or single geometric phase change at the given frequency f can be obtained through the dot product of these two state vectors and can be expressed as

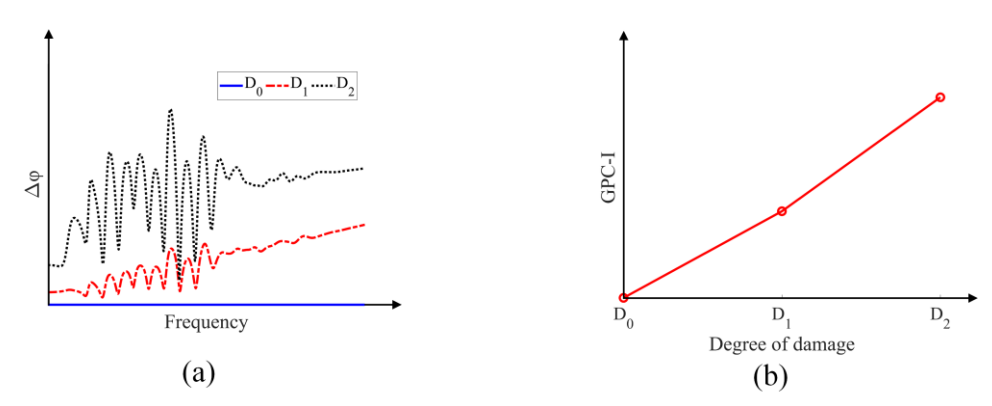
$$\Delta \varphi = \operatorname{arcos}(\operatorname{Re}(C * \cdot C')), \quad \Delta \varphi \in [0, \pi]$$
 (3)

where *C*\* denotes the complex conjugate of state vector *C* while Re stands for the real part of a complex quantity.

Generally, the acoustic signals at each receiving point contain multiple frequencies because input excitation signals own the bandwidth which contains multiple frequency components, then a series of geometric phase changes at each frequency component can be plotted as a function of frequency, as shown in Figure 2a, with different levels of damage ( $D_0$ —no damage,  $D_1$ —medium level of damage and  $D_2$ —higher level of damage). The spectral dependency of the GPC  $\Delta \varphi$  measures changes in the spatial characteristics of the acoustic field during the wave propagation due to perturbations—the larger the perturbations are in structures the higher the GPC values are in the plots. The GPC-index (GPC-I) is defined as the average value of each GPC curve in the frequency-dependent  $\Phi$ 

Sensors 2024, 24, x FOR PEER REVIEW (GPC-I) is defined as the average value of each GPC curve in the frequency-dependent by losts.

The GPC-I values for different degrees of damage in Figure 2a are shown in Figure 2b.



Figigur 2. 2a) (1) Jaxaplip lot of PPG lipts to b) bCPP initiale (CPPQ) I) at also foot always free and always ded structures.

From Figure, it is is calculated that days go developing lateratures are but detected the abouse eyatic parter energy. The distribution, which there is the other former experies parter parter

#### 3. Model Description and Numerical Modeling

# 3.1. Peri-Ultrasound and FEM Modeling for Cracked Geometry

As illustrated in Section 2, for TA sensing the vector representation of an acoustic field in an infinite dimensional Hilbert space can be compared for damage-free and damaged plates. However, for practical applications, a much smaller discretized n-dimen-

Sensors 2024, 24, 6552 5 of 17

## 3. Model Description and Numerical Modeling

## 3.1. Peri-Ultrasound and FEM Modeling for Cracked Geometry

As illustrated in Section 2, for TA sensing the vector representation of an acoustic field in an infinite dimensional Hilbert space can be compared for damage-free and damaged plates. However, for practical applications, a much smaller discretized n-dimensional subspace is considered to describe the acoustic field. In this investigation, this subspace is generated from seven receiving points (so n = 7) as shown in Figure 3. It should be noted that in TA sensing at least two receiving points are needed to reflect the spatial characteristics of the acoustic field. More receiving points improve the spatial resolution of the acoustic field and its geometry. Here, seven receiving points are distributed symmetrically about the *y*-axis, as shown in Figure 3a (without any cracks) and in Figure 3b (with one crack). The distance between two adjacent receiving points is set at 25 mm. The dimensions of the plate structure for numerical modeling are  $201 \times 201 \times 3$ mm<sup>3</sup>. The thickness d of the crack in Figure 3b takes values 0, 1, 2 and 4 mm for modeling damage growth in the plate and the length of the crack is fixed at 19 mm. A plate having no cracks is considered as the reference state or reference shape with respect to which the cracked plates (perturbed states) are compared. For wave propagation modeling, the vertical distances from the transmitting point and the seven receiving points to the x-axis are set at 60 mm. The crack is symmetrically placed about the y-axis with the bottom surface coinciding with the x-axis

Sensors 2024, 24, x FOR PEER REVIEWING the crack thickness increases as the top surface moves in the positive y direction. of the material properties considered for the numerical modeling are listed in Table 1.

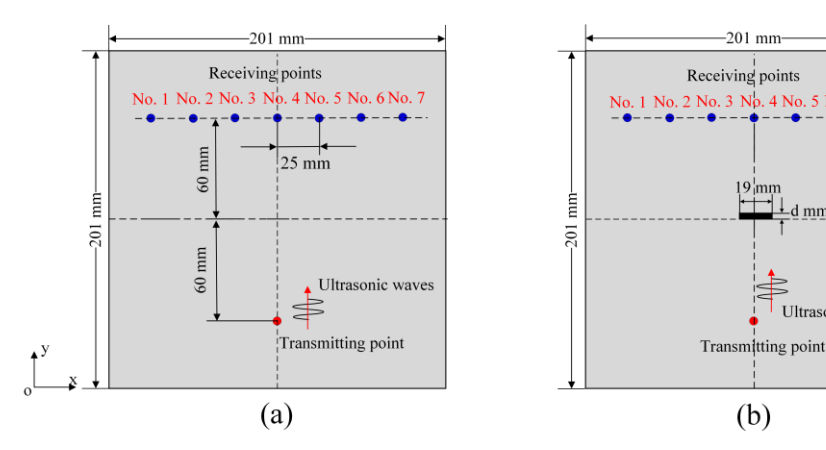


Figure 3: TWO additions singularly like with the probability generative for TA TA sensing clack free free plate creference setato) (backecked relate (nerturbed setate).

Table 1. Plate material properties for FEM and peri-ultrasound numerical modeling.

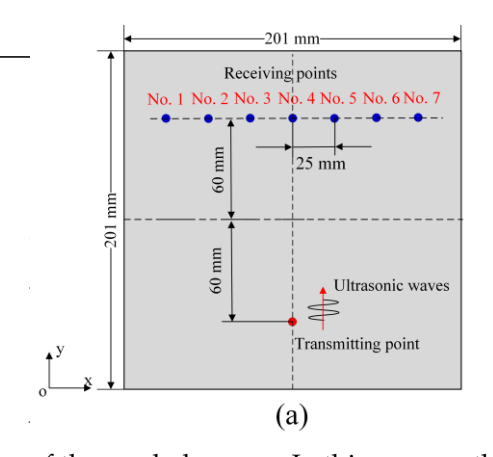
Par <b>ameter</b> er	Youngsangedudual(GPaPa)	Poisson on Ratioio	Density (laggni))
Values Values	$71.59_{1.50}$	0.3 <del>8</del> .33	2700000

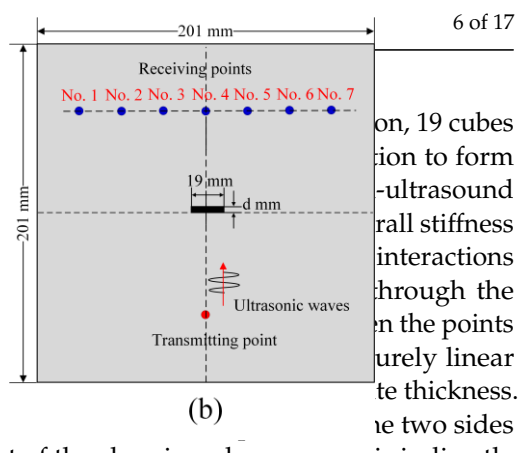
To arrive at a better understanding of how elastic waves propagate in the plate considered here, the phase velocity dispersion curves of a 3 mm thick aluminum plate are sidered here, the phase velocity dispersion curves of a 3 mm thick aluminum plate are computed using the material properties given in Table 1. Figure 4 shows the plots of phase computed using the material properties given in Table 1. Figure 4 shows the plots of phase and group velocity dispersion curves of the  $\S_0$  and  $\S_0$  guided wave modes in the plate, and group velocity dispersion curves of the  $\S_0$  and  $\S_0$  guided wave modes in the plate.

soon In the mesh-free peri-ultrasound modeling, the entire plate structure is discretized into cubes with side length of 1 mm. Therefore, 201 cubes are taken in the x direction for the problem geometry shown in Figure 3. The horizon size defined in peri-ultrasound modeling is selected as  $\delta = 3.015\Delta x$  following references [32–34] to ensure both computational efficiency and accuracy, where  $\Delta x$  is selected as 1 mm, which denotes the side length of the cube. All output variables are recorded on particles at receiving locations distributed symmetrically about the y-axis. Cracks are formed by removing one or more layers of

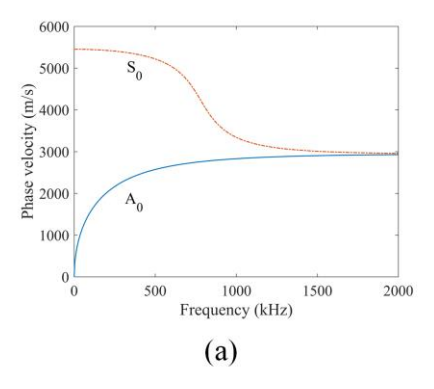
1000 1000 1500 2000 Frequency (kHz) Frequency (kHz) (b) (a)

Sensors 2024, 24, 6552





of the crack decrease. In this manner the effect of the clapping phenomenon is indirectly rigure 3. Two-dimensional view of the problem geometry for 1A sensing: (a) crack-free plate (recaptured since) the clapping of thin cracks allows more wave energy to pass through a thin crack compared to a thick crack. Thus, both peri-ultrasound modeling and the crack damping phenomenop which is also provided as contact acoustic nealinearity (CAN) [35–38] result in more interactions between the points on the two sides of the crack for thin cracks contact acoustic nealinearity (CAN) [35–38] result in more interactions between the points on the two sides of the crack for thin cracks contact acoustic nealing and the crack for thin cracks contact acoustic nealing are the points on the two sides of the crack for thin cracks contact acoustic nealing are the points on the two sides of the crack for thin cracks contact acoustic nealing on the horizon 74-50s mentioned in nonlocal periodynamics 25/2000 Here, in our peri-ultrasound modeling, the horizon size is 3.015 mm (with a 1 mm side length of the cibersiveraths better authorists as sides of the crack plate crack with radiation at the plate and contact and properties as a side of the contact acoust by inpute the contact and properties are also as a side of the contact acoust by inpute the contact acoust a side of the contact acoust account account and account account



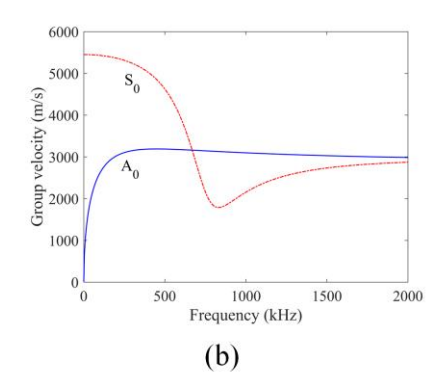


Figure 4. Dispersion curves for a 3 mm thick aluminum plate: (a) Phase velocity; (b) stroup velocity:

For both FEM and peri-ultrasound modeling, a Hanning window modulated excitation displacement field with a contraduction of 2016 Harand with two civeles disapplied ant the utransmitting energy to excite the pelaterature of the target in the target in the control of the contr the proper still be a structure is discretized into sinite whole plate structure is discretized into sinite elements. To ensure the computation and accuracy of the numerical model it is essential to modeling is selected as 0 = 3.0150 following references 132-34 to ensure both compudetermine and adopt the appropriate element size (L) and the integration time step ( $\Delta t$ ). These two parameters can be determined from Equations (4) and (5) [40] length of the cube. All output variables are recorded on particles at receiving locations distributed symmetrically about the y-axis. Gracks are formed by removing one or more layers of cubes from the plate structure. Note that for each removed layer in the y direct tion, 19 cubes are removed in the x direction and 3 such layers are removed in the z direction to form the through-thickness crack It should be emphasized that in the nonlocal peri-ultrasound modeling, the cracks are modeled by removing material cubes and thus the overall-stiffments recibe respire 2000 RTH the her admiral no wedge to of the many live the transfer is another interaction in between the aroung actives classification areas and cracks is called under restlycterbaigh the interaction trabot more placer at ental equipted located more than the integer demotes of add by Nichethian points is reducated as idn't as revitared as plin being separated revoluting authorized by signals is 50 MSa/s (mega samples per second) to ensure computation accuracy.

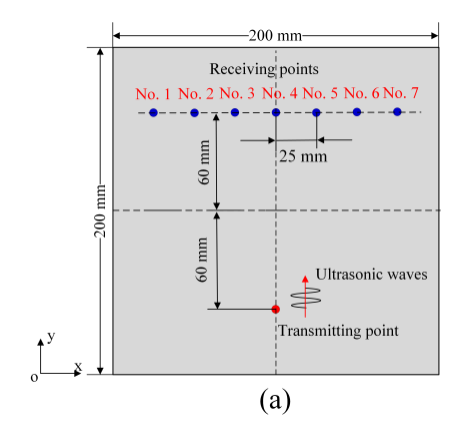
Sensors **2024**, 24, 6552 7 of 17

At the receiving points, velocity values (in the z direction or perpendicular to the plate surface) for each crack thickness are recorded at every calculation step to obtain the time history signal at each receiving point. Thus, seven signals are recorded at seven receiving points for every crack thickness: 0 mm (no crack), 1 mm, 2 mm and 4 mm. Then, GPC analysis is carried out with these signals.

#### 3.2. FEM Modeling for Material Nonlinearity Problems

The effect of material nonlinearity on GPC is investigated by FEM modeling. The 2-D view (the xy plane) of the problem geometry that is modeled is shown in Figure 5a. The dimensions of the plate structure are  $200 \times 200 \times 3 \text{mm}^3$ , the linear elastic material properties for numerical modeling are listed in Table 1 and the nonlinear material properties (stress–strain relationships) are prescribed in the Abaqus/CAE software. For wave propagation setup, the excitation point or the transmitting point is selected on the top surface of the plate, on the *y*-axis, and the seven receiving points are distributed symmetrically

Sensors 2024, 24, x FOR PEER REVIEW bout the *y*-axis. The vertical distance of the horizontal central axis of the plate from the figure.



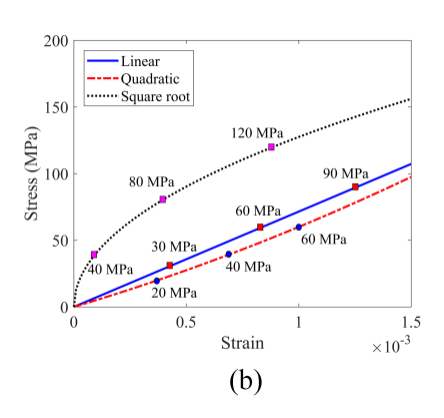


Figure 5. Two-dimensional view of the problems geneter of the legester setuence dates a strain relationships for wave propagation model is a large day of the segmentar (b) (by easest in an attentions.

ve different stress–strain relationships are considered for the numerical investigation we different stress–strain relationships are considered for the numerical investigarive different stress—strain relationships are considered for the numerical investiga-with FEM modeling. Figure 5b shows three of the five stress—strain relationships that are tion with FEM modeling. Figure 5b shows three of the five stress—strain relationships that considered. The middle solid line indicates a linear stress—strain relationship where the are considered. The middle solid line indicates a linear stress—strain relationship where stiffness remains constant; the lower dashed line gives a quadratic relationship be-stress and strain where the stiffness increases as the load increases; the top dotted line tween stress and strain where the stiffness increases as the load increases; the top dotted line shows in square root stress—strain relation ship where the stiffness decreases whe load increases a The three chumbers and keden teach surve are scribed heatness a militude awhen ten material inleade dialous the assume do troop attraction repete Everes dialous later seing ain ralationiships objected aboresidered but the babamidinothe figure. Three appredictaintress haing pappirtlemadda(i) hhe anibid ohe texinand (ii) hhit one thir deference straint The (anaplifiefætienceacture is Hhis ndiefineuthas thee; atiokon gha Excitațio grant plitbate 10 [acreference amplitude The3rDipletestructure is the cratized into value brankfrigite Platvents ignerated thous 19.728]. 2021 Fightwarp. Franky element harsa diderlength of homm runchediscretization opendunes 201 the Applepation through visit thus entities a termentities assist leasted on the restablies every alion Becaucies 201 intraes anther mederate, distributed symmetrically about the valeties of the enfransistent with y hat is achieved in the pericultrasound modeling described in Section 3 bout An explicit dynamic solution scheme is adopted for our calculation. The initial excitation is the y-axis. This is consistent with what is achieved in the pen-ultrasound modeling dethe y-exis. This is consistent with what is achieved in the peri-unitasound modeling de-applied to the transmitting point in the negative z direction, and the velocity values in the z scribed in Section 3.1. Afrexplicit dynamic solution scheme is adopted for our calculation, direction, perpendicular to the plate surface, are recorded at the seven receiving points for The initial excitation is applied to the transmitting point in the negative z direction, and geometric phase analysis. The sampling frequency at the receiving point is 50 MSa/s (mega the velocity values in the z-direction, perpendicular to the plate surface, are recorded at samples per second). For each stress-strain relationship shown in Figure 3b, there are three the seven receiving points for geometric phase analysis. The sampling frequency at the receiving point is 50 MSa/s (mega samples per second). For each stress–strain relationship shown in Figure 5b, there are three recorded signals which correspond to the AF values equal to 1, 2 and 3, respectively, at each receiving point, so a total of nine signals are recorded at each receiving point for the material nonlinearity analysis by the TA sensing

Sensors **2024**, 24, 6552 8 of 17

recorded signals which correspond to the AF values equal to 1, 2 and 3, respectively, at each receiving point, so a total of nine signals are recorded at each receiving point for the material nonlinearity analysis by the TA sensing technique.

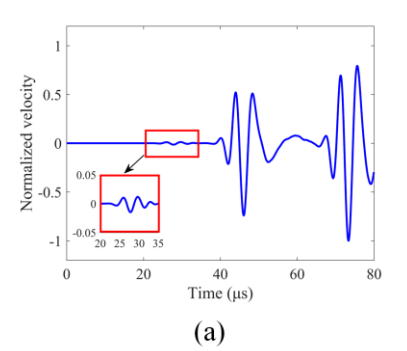
## 4. Numerical Modeling Results

## 4.1. Effects of FEM and Peri-Ultrasound Modeling on Wave Propagation

Both local FEM modeling and nonlocal peridynamics (PD)-based peri-ultrasound modeling are used to investigate the effect of crack initiation and growth on the wave propagation behavior and GPC calculation. In FEM modeling, the surfaces of cracks remain separated as the waves propagate, so elastic waves cannot pass through an open crack but are scattered by it. However, in nonlocal peri-ultrasound modeling, due to the nonlocal effect, waves can pass through a crack, so both linear and nonlinear responses are generated

Sensors 2024, 24, x FOR PEER REVIEW generated.

In the TA sensing technique the GPC parameter can theoretically sense both linear and nonlinear responses. However, separate as well as combined investigations of linear and nonlinear effects on GPC can provide guidance on the applicability of GPC for sensing micro-cracks (nonlinear responses). A comparison of the results of these two modeling techniques in terms of the geometric phase change (GPC) can help us to understand the effects of linear anti-nonlinear responses compared of First of order cracks concerned to the property of the results of the results of these two modeling techniques in terms of the geometric phase change (GPC) can help us to understand the effects of linear anti-nonlinear responses compared of the results of these two modeling. Nonlinear techniques in the control of the results of these two modeling. Nonlinear anti-nonlinear responses compared to the results of the results of these two modelings are the results of the results of these two modelings of the results of these two modelings. Nonlinear anti-nonlinear responses compared to the results of the results of these two modelings are responses to the results of the results of the results of the results of these two modelings.



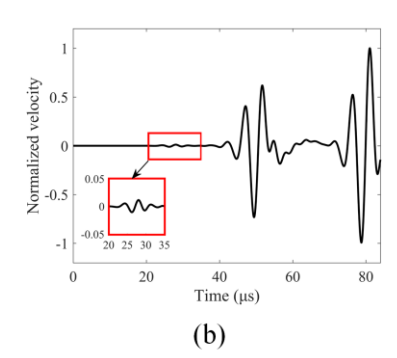


Figure 6: Normalized velocity-time-histopy-arrecieved for or never least normalized velocity-time-histopy-arrecieved for or never least never least never least the period of the period

For the no-crack case, it can be seen from Figure 6 that the two numerical modeling techniquen generate rimiler hesult but erenstrictly speaking untidoptical rime promodeliventechnique is have shount renant ocal the curi while that or be converient in the convertable eningerical modeling see thouse learly showed ifferent and the average modes. Where they are expressed to appear in the time chiatory about affording truthe dispersions where how his Experted teappear iron earneanisteric projection are committed the utilities on the very solution of the committee of the com rigues at receiver we can heave connocethicknesses (Ampune a results in the and Ampule generated by these two numerical modeling techniques are also compared, and shown in Figure 7 erated by these two numerical modeling techniques are also compared and shown in Figure generated from the cracks, there are significant changes between the no-crack case (0 mm thick crack) and the cracked cases (1 mm, 2 mm and 4 mm). However, there are almost no changes for 1 mm, 2 mm and 4 mm thick cracks (these three curves overlap). Therefore, it can be concluded that damage growth (the increase in thick thickness) does not significantly affect the pure linear scattering response. However for the peri-ultrasound modeling results shown in Figure 7b, where elastic waves can pass through the no-crack case as well as through some cracks (having 1 mm and 2 mm thicknesses) and to a lesser degree through the 4 mm thick crack [32,33], both linear and nonlinear responses are generated. The linear response is from the reflection, refraction and scattering of the waves by the crack's surface while the nonlinear response is from the nonlocal effects when some elastic

Time (μs)

(a)

Time (μs)

(b)

**Figure 7.** Normalized velocity time history at receiver 4 for four cases (0 mm or no-crack, 1 mm, 2 mm and 4 mm thick cracks) from two different numerical modeling techniques: (a) finite element method (FEM): (b) peridynamics (PD) based perioultrasound modeling

(a)

9 of 17

ateal/byer(e)-gipripasbess throughoth (FGEM) k(b) Liperiolytnastits (HLM) Invode bing ultrascrisull trasloting কিটোর্ট্যান্ত্র there are significant changes in time histories for 1 mm, 2 mm and 4 mm thick cracks. Since we have pointed out and concluded that in FEM modeling a purely linear scattern the sported cosmot dampe forest one is the session of the test of the cosmological cosm tackniqueaceanaertaesimilaraesultsibutaepoistrintlysepaakimeaantigaesianlsinaeraeanedo diestrahniquetedeschembertschen verteeldbeschen de de met de met de schemberteelde de de de de de de de de de d vincerical modeling prethological such show of Higrary guided. When mode to bake they dies exposited the preción that ime bistorated at ascerding tentre alidrasion divernations Sensors 2024, 24, x FOR PEER REVIE Digween Hanne, internal have comfidence in ouncomputation with the sensors 2024, 24, x FOR PEER REVIE Digween Hanne, internal have comfidence in ouncomputation. viduosatorekoi vieto A. Ton tilhe tiinnechisto this Ishessas i(0) Filgurt Tribo thamidadt 4 mdn): gentad atead desymblycent word tubunce niffed in tubed e beeg teal blotty slow wire and stig corre particles and collection by a fine of the large way and the contraction of the contraction o The viole a dietopious is not direct ne next shifts as the creak thick some increases throw detail mine. crack's surface while the nonlinear response is from the nonlocal effects when some elastic wave energy passes through the cracks. In contrast to FEM modeling, in peri-ultrasound modeling there are significant changes in time histories for 1 mm, 2 mm and 4 mm thick ceacks. Since we have pointed out and concluded that in FEM modeling a purely linear scattering response does not change when crack thickness increases, the changes observed due to crack thickness variations in the perialitrasound modeling result must be due to the nonlinear effects generated by the cracks. The effect of damage growth (the increase in crack thickness) on spectral plots is shown in Figures 8 and 9. The multiple peaks and

dips shown in the spectral plots are generated by the constructive and destructive interferences between the incident wave from the source and the reflected wave from the boundary at the sensor location. In the time histories shown in Figure 7, both incident and reflected waves appear and thus affect the spectral plot shown in Figure 8. The spectral plot shown in Figure 8.

Figure 6. Normalized velocity time history at receiver 4 for no-crack case (0 mm thick crack) gener-

1.2

— No crack
— 1 mm thick crack
— 2 mm thick crack
— 4 mm thick crack
— 4 mm thick crack
— 4 mm thick crack
— 7 mm thick crack
— 8 mm thick crack
— 9 mm thick crack
— 9 mm thick crack
— 1 mm thick crack
— 2 mm thick crack
— 1 mm thick crack
— 2 mm thick crack
— 1 mm thick crack
— 2 mm thick cra

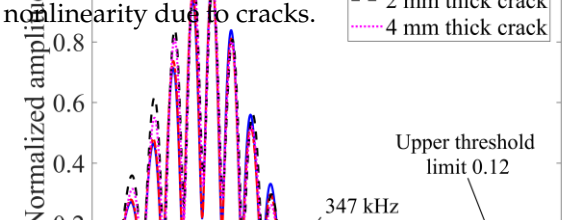
inethold (FEM), (b) peridynamics (PD)-based peri-ultrasound modeling.

a, where only linear scattering is genes between the no-crack case (0 mm 4 mm). However, there are almost no se three curves overlap). Therefore, it e in crack thickness) does not signifiwever, for the peri-ultrasound model-can pass through the no-crack case as m thicknesses) and to a lesser degree id nonlinear responses are generated.

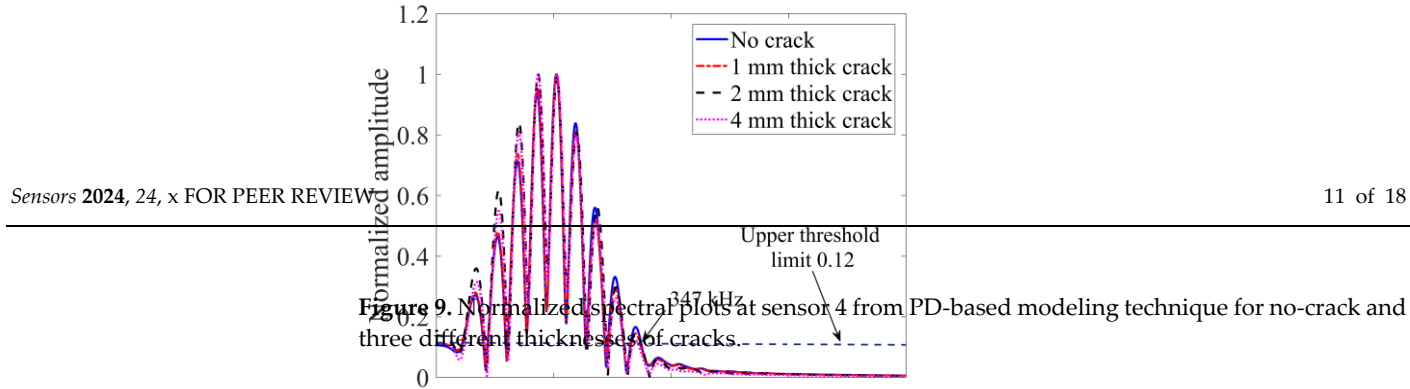
Figure 8. Nonnmallized spectral photos at ecceivine 4 from FFNE Modeling in the input for oracle askecased and electrified in the third control of the contr

For the purely linear scattering response in FEM shown in Figure 8, there is almost no change on the spectral envelope shape for the four cases, indicating that no additional frequency components are generated. Also, there are no differences for the three crack thicknesses (1, 2 and 4 mm). This clearly proves that the crack thickness increase does not affect the purely linear scattering from cracks.

In the peri-ultrasound modeling results shown in Figure 9, it can be observed that the envelopes for 2 mm and 4 mm thick cracks are distorted (the 1 mm thick crack case is also slightly distorted compared to the no-crack case). Therefore, additional frequency components are generated. Such additional frequency components indicate the presence of



For the purely linear scattering response in FEM shown in Figure 8, there is almost no change on the spectral envelope shape for the four cases, indicating that no additional frequency components are generated. Also, there are no differences for the three crack thicknesses (1, 2 and 4 mm). This clearly proves that the crack thickness increase dods not affect the purely linear scattering from cracks.

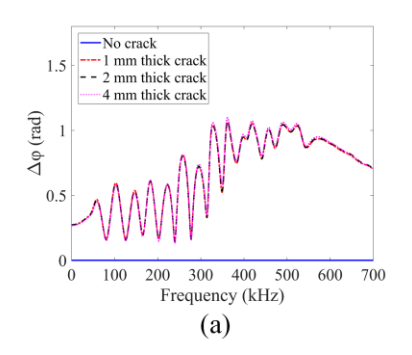


In the per2011trasour (10 modeling) results (10 mm in Figure 9, it can be observed that the envelopes for 2 from (14 mm) thick cracks are distorted (the 1 mm thick crack case is also slightly distorted compared to the no-crack case). Therefore, additional frequency Figure 9. Normalized spectral plots at sensor 4 from PD-based modeling technique for no-crack and components are generated. Such additional frequency components indicate the presence three different thicknesses of gracks.

The nonlinear behaviors from the cracks are also analyzed with the help of the side-band peak count-index (or SPC-I) parameter. We took the upper the shold thin it the zion tal-deshid in the beginning of the side band peak count-index (or SPC-I) parameter. We took the upper the shold thin it the zion tal-deshid in the shold in the side of the side o

## 4.2. GPC Computation for Damage Growth

Im this section, GPC which is from the TA-sensing methodology reretioned in 6-bettion is is really by the two numerical modeling techniques are obtained and shown im Figure 10.



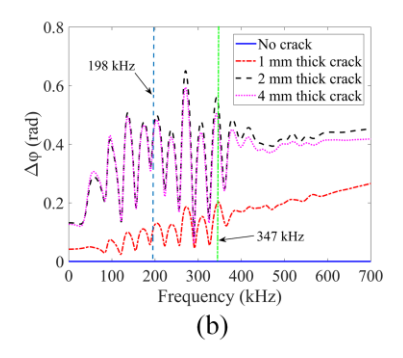


Figure 10. Crack effects on GPC calculation obtained from two different numerical modeling techniques: (a) FEM modeling; (b) peri-ultrasound modeling.

For the purely linear scattering response, it is not be seen of that that the fauthey credended to the seen sitily of othe crack appearing in the structure—multiple sharp peaks and dips can be observed for the cracked plates. However, no measurable changes are noticed when crack thickness increases from 1 mm to 4 mm. Therefore, the inear scattering response of PGP is no honselved to a magning with Julian prie ultrashind—modeling response of PGP is no honselved to a magning with Julian prie ultrashind—modeling resulting heavily shown in Figure 100 plots beginning and some cracks. Clear differences are observed when crack thickness increases (indicating damage caused by the cracks. Clear differences are observed when observed when crack thickness increases (indicating damage growth). At the higher frequency ranges beginning from about 198 kHz (the first vertical dashed line in Figure 10b), the CPC plots beginning from about 198 kHz (the first vertical dashed line in Figure 10b), the CPC plots begin to show a triend which is the trend observed in the lower frequency range (below 100 kHz). At lower frequencies, the peak values in Figure 10b increase with crack thickness but at higher frequencies (above 198 kHz) the peak values first increase for crack thicknesses up to 2 mm and then decrease. The higher frequency trend is consistent with previous investigations with SPC-I [18,38–40] where it was shown that the nonlinear parameter SPC-I value first increases and then decreases with damage growth. Since the SPC-I technique mainly cap-

Sensors **2024**, 24, 6552

nonlinearity (CAN) and the SPC-I value increases. When these micro-cracks coalesce to form macro-cracks, the crack surfaces do not come into contact to generate nonlinearity and their SVGTL value righter sets. Therefore with Crack capture as nonlinear gresponse due to damage growth) when it is calculated at the appropriate frequency est should be noted that atchigher frequencies the wavelength is smallete. When the crack thickness increases from 7 mgsto 4 granter a continuar contractor of the to a maller revealers that he amagide not the stacke the strength and the applies ene eftertiketi-itelswerstreaussgist with darrage avelan set ethekude. The permetized SPA-Invariations twith igner presentates hold this it infall the case taked wear liet a are relatinged chararismalnet receives the unimeches and season recient modeling techniques a Trouble descriptions anterbowners intervalor (the first column in things earling contact acoustic nonlinearity (CAN) harge threst ic phate charge indewhen GRE Initial time its established was invalue of whole ARC plots surfacted GRG plots was certain frequency cannot be quantificated and the Stick patte decreased Phylogory GPC main apterest. Flugline allegives the legions of the regularity of the pattern of caharlaiting takeGRCed valute. At bigbeiakequencangus stromation and tess that at higher frequencies atheistente britg the SSPG all on riAften tibe of Adle thickness your ergs of some 192 labla tth4 first, vtrticadrdisseadrlisseansEiglacceltSes to 7900 laHerisvaveliderttes to Tobisaint 620 devider sussaften with rective options the ideal on side sing the language of a modified GRCF-lovge intrinsis thre about meinr Effected 11 that I three conficency in the language was elementated three SPE-three and is a conficency in the specific of the transportations vaidy autropop 6.4 Phk et halth dissistant of the distribution of the second of the sittered verobusing Pase-tween sweeted modeling steal miquesting te APG alvertation Pase vhorations Figure 11c, f (the third column).

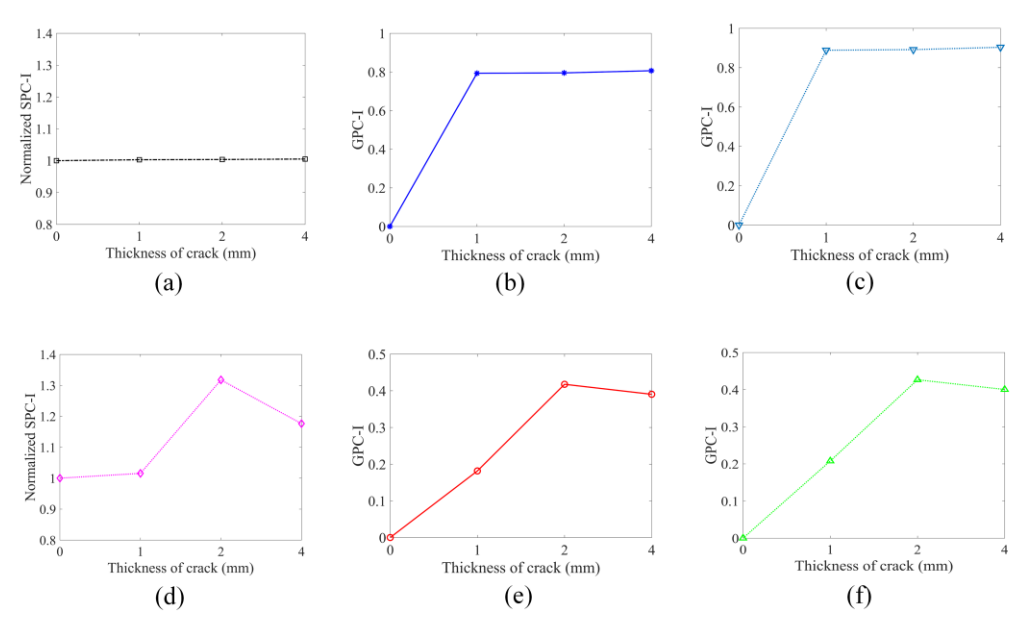


Figure 11. Variations in the crack thickness effects on SPC-I (the first column) and GPC-I (the second and third columns). The second column is calculated by arking at briteguency ranger from \$981 kHz to 700 kHz, and the third column is calculated in the frequency range of \$4.7 kHz to 700 kHz for proper proper comparison with the SPC-I values. The FEM (the top row) and the peri-ultrasound (the bottom row) results capture the linear response and the combined linear and nonlinear responses, respectively.

The geometric phase change-index (or GPC-I) is defined as the average value of whole It can be seen from the FEM modeling results (the top row in Figure II), that the GPC plots or partial GPC plots over certain frequency ranges depending on which parts of normalized SPC-I value which mainly captures the no linear response in strictures each GPC plots are our main interest. Figure 10b gives the frequency range for calculating shows almost no variation in Figure 11a, confirming that in FFM randeling only a linear the GPC-I values. At higher frequency ranges, from anothing 198 kHz, the GPC frequency ranges is generated. The GPC-I results can detect the formation of a crack of consistent with the SPC-I variation trend. The frequency range from 198 kHz (the first damage) but cannot mention crack growth size in Figure 11b, calmost a lovizous from the obtained as the crack this kness changes. In the peri-ultrasound modeling results (the bottom now in Figure 11), both GPC-I and SPC-I variations are shown in Figure 11b, the first of proper comparison with the SPC-I results, a second required to range from 347 kHz (the second vertical line in Figure 10b) to 700 kHz is considered to

Sensors **2024**, 24, 6552 12 of 17

obtain GPC-I values from the two numerical modeling techniques. The GPC-I variations obtained from this analysis are shown in Figure 11c,f (the third column).

It can be seen from the FEM modeling results (the top row in Figure 11), that the

normalized SPC-I value which mainly captures the nonlinear response in structures shows almost no variation in Figure 11a, confirming that in FEM modeling only a linear scattering Sensors 2024, 24, x FOR PEER REVIEWESPONSE is generated. The GPC-I results can detect the formation of a crack (or damage) but cannot monitor crack growth since in Figure 11b,c almost a horizontal line is obtained as the crack thickness changes. In the peri-ultrasound modeling results (the bottom row in Figure 11), both GPC-I and SPC-I show consistent trends—first increasing up to 2 mm to 2 mm and then decreasing, thus forming a hump In several experimental and theoretical retical investigations that the peri-ultrasound modeling results (the bottom row in Figure 11), both GPC-I and SPC-I show consistent trends—first increasing up to 2 mm to 2 mm to 2 mm to 2 mm to 3 mm several experimental and theoretical retical investigations of this forming a hump Interest in the several experimental and theoretical retical investigations in the properties of the properties of

## 4.3. GPC Computation for Material Nonlinearity

The investigations of the effect of material nonlinearity on GPC were carried out with FEM modeling in the Abaqus/CAE softtware. The mormalized spectral plots, obtained from the recorded time histories at receiver 4 for three different stress—strain relationships are shown in Figure 12. The normalized curves are plotted in a logarithmic scale to provide a clear understanding of how sideletrad possishanges is proparcitations in strategistic band parallitude in the response is linear or nonlinear [26]. For linear responses, the normalized plots should not show any difference but for nonlinear responses the normalized plots should not show any difference but for nonlinear responses the normalized plots should show some difference when the applications of the control of the plants of the plots of the plants of the plots of the plants of the plants

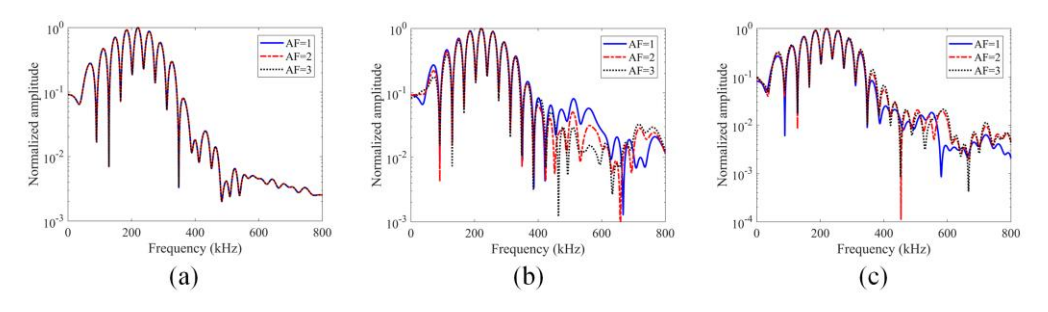


Figure 12. Normalizeds ppetural plate to constant about market in the figure 12. Normalizeds ppetural plate to constant about market in the figure of the figure in the figure of the figure is a strain at lation of the figure in the figure is a strain at lation of the figure is a strain at lation at la

It can be seen in Figure 12a than in the same and another finding restress at the rational peaks (which are timber any yrism the control frequency of 200 kHz) and the sideband peaks (which are timber any yrism through kHz control frequency of 200 kHz) and the sideband peaks (which are timber any yrism through kHz control frequency of 200 kHz) and the sideband peaks (which are timber any rism through the sideband satisfies the rational stress the main lobe annititudes in the normalizated of the southers by the sideband bank peak tamplitudes are rises. Sintly surface trains elationship the sideband peak amplitude values. Similarly, for square root stress—strain relationships, as can be seen in Figure 12c, the sideband peaks also show nonlinearly—this time, the sideband peak amplitudes increase as the AF increases while the main lobe amplitudes remain unchanged in the normalized plots. The GPC plots for these three types of materials are shown in Figure 13. Figure 13a—c correspond to linear,

Sensors **2024**, 24, 6552 13 of 17

produces lower sideband peak amplitude values. Similarly, for square root stress–strain relationships, as can be seen in Figure 12c, the sideband peaks also show nonlinearly—this time, the sideband peak amplitudes increase as the AF increases while the main lobe amplitudes remain unchanged in the normalized plots. The GPC plots for these three sensors 2024, 24, x FOR PEER REVIEW pees of materials are shown in Figure 13. Figure 13a–c correspond to linear, quadratic and

square root stress-strain relationships, respectively.

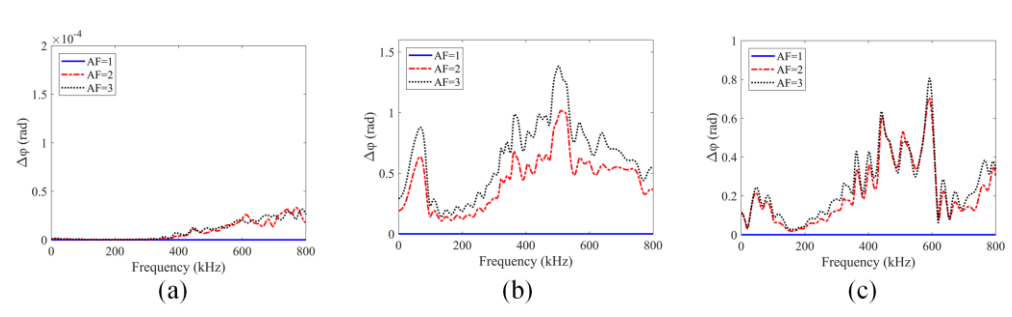
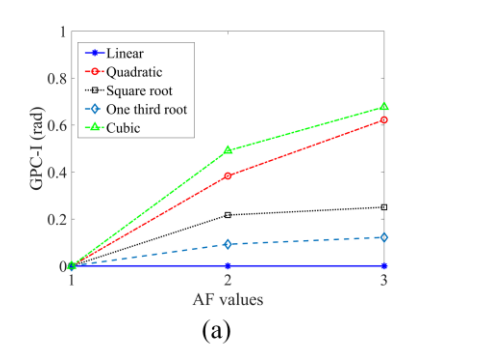
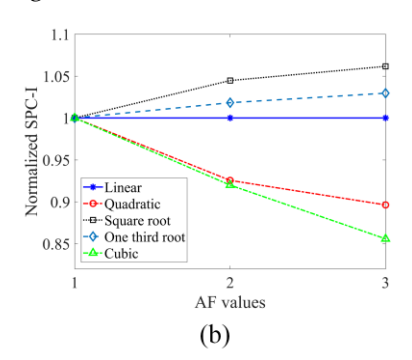


Figure 13. Cometriciphase change variations for different stress strain relationships: (a) linear; (b); the different stress strain relationships: (a) linear; (b); the different stress strain relationships: (b); the different stress strain relationships: (b);

The sear from Figure 13 that for linear stress strain relationships the EFC plots show no changes as input excitations increase from 1900 anound 300 kHz. However, some small non-zero values at higher frequencies from approximately 300 kHz to 800 kHz are observed. Theoretically, for linear stress-strain relationships; there should be not change in the mornalized plots when input excitations increase as shown in Figure 122 (the time band peaks do not show any changes). These oscillations cannot be smaller wavelengths) are modeled. Also, random noise from turn cations in the maximum magnitudes of these oscillations are around 3 × 103 rad at 800 kHz which is almost zero in comparison to the scale (100) of Figure 136. Therefore, those very small values can be removed and assumed to be scale (100) of Figure 136. Therefore, those very small values can be removed and assumed to be scale (100) of Figure 136. Therefore, those very small values can be removed and assumed to be scale (100) of Figure 136. Therefore those very small values can be removed and assumed to be scale (100) of Figure 136. Therefore those very small values can be removed and assumed to be scale (100) of Figure 136. Therefore those very small values can be removed and assumed to be scale (100) of Figure 136. Therefore those very small values can be removed and assumed to be scale (100) of Figure 136. Therefore those very small values can be removed and assumed to be scale (100) of Figure 136. Therefore those very small values can be removed and assumed to be scale (100) of Figure 136. Therefore those very small values can be removed and assumed to be scale (100) of Figure 136. Therefore those very small values can be removed and assumed to be scale (100) of Figure 136. Therefore those very small values can be removed and assumed to be scale (100) of Figure 136. Therefore the provide the figure 136. Therefore the provide the provide the figure 136. Therefore the provide the provide the figure 136. Therefore the provide the provide the provide the prov





Higure 14. (a) Geometric phase change index (CPC-I); (b) normalized SPC-I variations for material regure 14. (a) Geometric phase change index (CPC-I); (b) normalized SPC-I variations for material modificative for different stress—strain relationships.

It can be seen from the GPC In lots in Figure 14a that for linear stress is train, relationships of C1 values do not change as input excitations increase, while for the other two nonlinear materials GPC-1 values increase as input excitations increase. For the SPC-1 plots shown in Figure 14b, for the linear material, SPC-1 values do not change as input excitations increase, which is consistent with what the GPC-1 plots show. However, for the other two nonlinear stress-strain relationships—quadratic and square root—the SPC-1 plots show two opposite trends for the two types of nonlinearities. When input excitations increases, which is consistent with what the GPC-1 plots show the SPC-1 plots show the stress-strain relationships—quadratic and square root—the SPC-1 plots show two opposite trends for the two types of nonlinearities. When input excitations in-

Sensors **2024**, 24, 6552 14 of 17

two nonlinear materials GPC-I values increase as input excitations increase. For the SPC-I plots shown in Figure 14b, for the linear material, SPC-I values do not change as input excitations increase, which is consistent with what the GPC-I plots show. However, for the other two nonlinear stress-strain relationships—quadratic and square root—the SPC-I plots show two opposite trends for the two types of nonlinearities. When input excitations increase, an increasing trend is observed for the square root stress-strain relationship while a decreasing trend is found for the quadratic stress-strain relationship. Such differences between GPC-I and SPC-I variations for nonlinear materials can be explained in the following manner. GPC-I shows the degree of deviations between the perturbed system (when AF is not equal to 1 in linear and nonlinear materials) and the reference system (AF = 1). Both quadratic and square root stress-strain relationships lead to perturbations from the reference state. The GPC-I senses and plots higher differences for higher AF values. In the SPC-I technique, the variations are related to the sideband peaks' amplitudes, which are linked to the stiffness of the material. When the stiffness of the material increases with strain (in the quadratic case), the generated nonlinear strain levels for the same stress levels become smaller, thus causing lower sideband peak amplitudes. When the stiffness of the material decreases with strain (in the square root case), the generated strains for the same stress level become larger, thus causing higher sideband peak amplitudes. In addition to the three stress-strain relationships discussed above, two more (one-third root and cubic stress-strain relationships) are analyzed. The SPC-I and GPC-I variations for all five cases are shown in Figure 14. The expected trends are observed: the one-third root relationship is similar to the square root relationship (since here material stiffness decreases as excitation increases), and the cubic relationship is similar to the quadratic relationship (since here material stiffness increases as excitation increases). Both the GPC-I and SPC-I variations could distinctly separate the five different stress-strain behaviors of the material. It can be also concluded from Figure 14 that SPC-I is more effective for distinguishing between different types of material nonlinearity than GPC-I. From the SPC-I plots (noticing whether the variation has an upward or a downward trend) one can say whether the material stiffness increases or decreases when the excitation amplitude increases which is not possible from the GPC-I plots.

## 5. Conclusions

In this work, a numerical investigation is carried out to compare the effects of damage initiation, damage growth and the change in material nonlinearity on the nonlinear ultrasonic technique SPC-I and the TA sensing technique GPC-I. Damage growth (increasing crack thickness) problems are modeled by two numerical techniques—the local finite element method (FEM) and the nonlocal peridynamics (PD)-based peri-ultrasound modeling technique. The effectiveness of the FEM and peri-ultrasound techniques in terms of modeling wave propagation in nonlinear and linear materials in the presence or absence of cracks is also investigated in depth. In FEM modeling, the surface of cracks is not artificially changed. No compressive or shear springs are placed inside the crack, unlike the case in some FE-based models to represent partially closed cracks. Thus, elastic waves cannot pass through an open crack and only purely linear scatterings are generated. However, in nonlocal peri-ultrasound modeling, due to the nonlocal effect, the elastic waves can pass through cracks so both linear and nonlinear responses are generated. A new acoustic parameter called the geometric phase change- index (or GPC-I), which is generated from TA sensing, is defined and adopted to monitor damage growth and material nonlinearity. In damage growth problems, the numerical results show that, for a linear response generated by FEM modeling, the GPC-I is sensitive enough to detect defects but cannot monitor damage growth. In the combined linear and nonlinear responses generated by peri-ultrasound modeling, at the higher frequency range, the GPC-I and SPC-I techniques show consistent trends—first increasing and then decreasing as damage grows. These results indicate that GPC-I can be used to detect the initiation of damage in structures from the linear analysis. From the combined linear/nonlinear analysis, it is shown that GPC-I

Sensors **2024**, 24, 6552 15 of 17

can also be used effectively to monitor damage growth by selecting only the higher frequencies in the analysis. The higher frequency boundaries are selected from the GPC plots. Recently, using a scanning laser doppler vibrometer (LDV), experimental investigation has been carried out to see if GPC-I and SPC-I can detect and monitor damage growth [43]. In this experimental investigation, the submillimeter indentations served as surrogates for flaws/defects. Similar to the numerical predictions in the current paper, in the experimental paper it was shown that the variations in the geometric phase and the SPC-I in the vicinity of the indentations are significant. The magnitudes of the variations in geometric phase and SPC-I have been shown to be strongly dependent on the number of indentations, i.e., on the level of damage to the plate.

The effect of pure material nonlinearity on GPC (in the absence of any cracks) is investigated by FEM modeling. Different stress-strain relationships—linear and nonlinear are considered. The numerical results show that for linear materials the GPC-I obtained from the normalized plots does not change as the input excitation increases while for nonlinear materials—with quadratic and square root stress-strain relationships (as well as for cubic and one-third root stress-strain relationships) the GPC-I increases as the input excitations increase, which indicates that nonlinear material behavior can be detected by the GPC-I technique. SPC-I analysis is also carried out for the same nonlinear materials. For linear, square root and one-third root stress-strain relationships, SPC-I shows consistent trends with GPC-I plots. However, for quadratic and cubic stress-strain relationships, SPC-I shows a decreasing trend as input excitations increase, which is the opposite of the GPC-I trends. This is because GPC-I measures the degree of deviations from the reference state (the linear material), and any perturbations introduced into the reference state can result in an increase in GPC-I values. The SPC-I technique, on the other hand, measures the number and strength of sideband peaks generated due to nonlinearity. The material's nonlinearity causes the stiffness changes with loading. Such stiffness changes affect the amplitudes and the number of sideband peaks. Therefore, SPC-I can capture trends in the change in material stiffness—whether increasing or decreasing with the excitation amplitude. For quadratic and cubic materials, the SPC-I shows a downward trend as load increases, while for square root and one-third root stress-strain relationships, the SPC-I shows an upward trend as load increases. Thus, the SPC-I technique can not only detect material nonlinearity but can also distinguish between types of nonlinearity. From its variation it can identify whether the material stiffness increases or decreases with increasing strain.

**Author Contributions:** Conceptualization, T.K. and P.A.D.; methodology, T.K. and P.A.D.; software, G.Z.; validation, G.Z.; formal analysis, G.Z.; investigation, G.Z. and K.R.; data curation, G.Z.; writing—original draft preparation, G.Z.; writing—review and editing, T.K., P.A.D., and K.R.; visualization, G.Z.; supervision, T.K. and P.A.D.; project administration, P.A.D.; funding acquisition, P.A.D. All authors have read and agreed to the published version of the manuscript.

**Funding:** This work was partially supported by the National Science Foundation sponsored "New Frontiers of Sound Science and Technology Center" at the University of Arizona (Grant No. 2242925).

**Institutional Review Board Statement:** Not applicable.

Informed Consent Statement: Not applicable.

Data Availability Statement: The dataset is available on request from the authors.

**Conflicts of Interest:** The authors declare no conflicts of interest.

#### References

1. Kot, P.; Muradov, M.; Gkantou, M.; Kamaris, G.S.; Hashim, K.; Yeboah, D. Recent advancements in non-destructive testing techniques for structural health mon-itoring. *Appl. Sci.* **2021**, *11*, 2750. [CrossRef]

- 2. Pallarés, F.J.; Betti, M.; Bartoli, G.; Pallarés, L. Structural health monitoring (SHM) and Nondestructive testing (NDT) of slender masonry structures: A practical review. *Constr. Build. Mater.* **2021**, 297, 123768. [CrossRef]
- 3. Zhang, G.; Li, X.; Li, T.; Kundu, T. Monitoring elastoplastic deformation in ductile metallic materials using sideband peak count-index (SPC-I) technique. *J. Nondestruct. Eval. Diagn. Progn. Eng. Syst.* **2023**, *6*, 1–15.

Sensors **2024**, 24, 6552 16 of 17

4. Park, S.; Alnuaimi, H.N.; Hayes, A.; Sitkiewicz, M.; Amjad, U.; Muralidharan, K.; Kundu, T. Nonlinear Acoustic Technique for Monitoring Porosity in Additively Manufactured Parts. *J. Nondestruct. Evaluation, Diagn. Progn. Eng. Syst.* 2022, *5*, 021008. [CrossRef]

- 5. Park, S.H.; Kundu, T. A modified sideband peak count based nonlinear ultrasonic technique for material characterization. *Ultrasonics* **2023**, *128*, 106858. [CrossRef]
- 6. Lata, T.D.; Deymier, P.A.; Runge, K.; Clark, W. Topological Acoustic Sensing Using Nonseparable Superpositions of Acoustic Waves. *Vibration* **2022**, *5*, 513–529. [CrossRef]
- 7. Liu, Y.; Song, Y.; Li, X.; Chen, C.; Zhou, K. Evaluating the reinforcement content and elastic properties of Mg-based composites using dual-mode ultrasonic velocities. *Ultrasonics* **2017**, *81*, 167–173. [CrossRef]
- 8. Zhang, G.; Liu, X.; Li, X.; Song, Y.; Zhang, S. Measurement of shear wave attenuation coefficient using a contact pulse-echo method with con-sideration of partial reflection effects. *Meas. Sci. Technol.* **2019**, *30*, 115601. [CrossRef]
- 9. Zhang, G.; Li, X.; Zhang, S.; Kundu, T. Investigation of frequency-dependent attenuation coefficients for multiple solids using a reliable pulse-echo ultrasonic measurement technique. *Measurement* **2021**, *177*, 109270. [CrossRef]
- 10. Li, X.; Yang, J.; Zhang, G. A Crack Size Quantification Method Using High-Resolution Lamb Waves. *Sensors* **2021**, *21*, 6941. [CrossRef]
- 11. Marino, D.; Kim, J.-Y.; Ruiz, A.; Joo, Y.-S.; Qu, J.; Jacobs, L.J. Using nonlinear ultrasound to track microstructural changes due to thermal aging in modified 9%Cr ferritic martensitic steel. *NDT E Int.* **2016**, *79*, 46–52. [CrossRef]
- 12. Doerr, C.; Kim, J.-Y.; Singh, P.; Wall, J.J.; Jacobs, L.J. Evaluation of sensitization in stainless steel 304 and 304L using nonlinear Rayleigh waves. *NDT E Int.* **2017**, *88*, 17–23. [CrossRef]
- 13. Thiele, S.; Kim, J.-Y.; Qu, J.; Jacobs, L.J. Air-coupled detection of nonlinear Rayleigh surface waves to assess material nonlinearity. *Ultrasonics* **2014**, *54*, 1470–1475. [CrossRef]
- 14. Donskoy, D.M.; Sutin, A.M. Vibro-Acoustic Modulation Nondestructive Evaluation Technique. *J. Intell. Mater. Syst. Struct.* **1998**, 9,765–771. [CrossRef]
- 15. Duffour, P.; Morbidini, M.; Cawley, P. A study of the vibro-acoustic modulation technique for the detection of cracks in metals. *J. Acoust. Soc. Am.* **2006**, *119*, 1463–1475. [CrossRef]
- 16. Van Den Abeele, K.E.A.; Johnson, P.A.; Sutin, A. Nonlinear elastic wave spectroscopy (NEWS) techniques to discern material damage, part I: Nonlinear wave modulation spectroscopy (NWMS). *J. Res. Nondestruct. Eval.* **2000**, *12*, 17–30. [CrossRef]
- 17. Van Den Abeele, K.E.A.; Carmeliet, J.; Ten Cate, J.A.; Johnson, P.A. Nonlinear elastic wave spectroscopy (NEWS) techniques to discern material damage, Part II: Single-mode nonlinear resonance acoustic spectroscopy. *J. Res. Nondestruct. Eval.* **2000**, *12*, 31–42. [CrossRef]
- 18. Alnuaimi, H.; Amjad, U.; Russo, P.; Lopresto, V.; Kundu, T. Monitoring damage in composite plates from crack initiation to macro-crack propagation combining linear and nonlinear ultrasonic techniques. *Struct. Heal. Monit.* **2021**, 20, 139–150. [CrossRef]
- 19. Alnuaimi, H.; Amjad, U.; Park, S.; Russo, P.; Lopresto, V.; Kundu, T. An improved nonlinear ultrasonic technique for detecting and monitoring impact induced damage in composite plates. *Ultrasonics* **2022**, *119*, 106620. [CrossRef]
- 20. Alnuaimi, H.N.; Sasmal, S.; Amjad, U.; Nikvar-Hassani, A.; Zhang, L.; Kundu, T. Monitoring Concrete Curing by Linear and Nonlinear Ultrasonic Methods. *ACI Mater. J.* **2022**, *118*, 61–69. [CrossRef]
- 21. Basu, S.; Thirumalaiselvi, A.; Sasmal, S.; Kundu, T. Nonlinear ultrasonics-based technique for monitoring damage progression in reinforced concrete structures. *Ultrasonics* **2021**, *115*, 106472. [CrossRef] [PubMed]
- 22. Park, S.; Bokhari, I.; Alnuaimi, H.; Amjad, U.; Fleischman, R.; Kundu, T. Early detection of steel tube welded joint failure using SPC-I nonlinear ultrasonic technique. *Struct. Heal. Monit.* **2024**, 14759217241235057. [CrossRef]
- 23. Arumaikani, T.; Sasmal, S.; Kundu, T. Detection of initiation of corrosion induced damage in concrete structures using nonlinear ultrasonic techniques. *J. Acoust. Soc. Am.* **2022**, *151*, 1341–1352. [CrossRef] [PubMed]
- 24. Castellano, A.; Fraddosio, A.; Paparella, F.; Piccioni, M.D.; Kundu, T. The evaluation of the adhesion defects in FRCM reinforcements for masonry constructions by Sideband Peak Count based nonlinear acoustic technique. *J. Vib. Control.* 2023. [CrossRef]
- 25. Wang, M.; Pau, A.; Zhang, G.; Kundu, T. Monitoring prestress in plates by sideband peak count-index (SPC-I) and nonlinear higher harmonics techniques. *Nonlinear Dyn.* **2023**, *111*, 15749–15766. [CrossRef]
- 26. Zhang, G.; Hu, B.; Alnuaimi, H.; Amjad, U.; Kundu, T. Numerical modeling with experimental verification investigating the effect of various nonlinearities on the sideband peak count-index technique. *Ultrasonics* **2024**, *138*, 107259. [CrossRef]
- 27. Lata, T.D.; Deymier, P.A.; Runge, K.; Le Tourneau, F.-M.; Ferrière, R.; Huettmann, F. Topological acoustic sensing of spatial patterns of trees in a model forest landscape. *Ecol. Model.* **2020**, *419*, 108964. [CrossRef]
- 28. Lata, T.D.; Deymier, P.A.; Runge, K.; Ferrière, R.; Huettmann, F. Topological acoustic sensing of ground stiffness: Presenting a potential means of sensing warming permafrost in a forest. *Cold Reg. Sci. Technol.* **2022**, 199, 103569. [CrossRef]
- 29. Hasan, M.A.; Deymier, P.A. Modeling and simulations of a nonlinear granular metamaterial: Application to geometric phase-based mass sensing. *Model. Simul. Mater. Sci. Eng.* **2022**, *30*, 074002. [CrossRef]
- 30. Lata, T.D.; Deymier, P.A.; Runge, K.; Uehara, G.S.; Hodges, T.M.W. Underwater acoustic sensing using the geometric phase. *J. Acoust. Soc. Am.* **2023**, 154, 2869–2877. [CrossRef]
- 31. Zhang, G.; Deymier, P.A.; Runge, K.; Kundu, T. Monitoring damage growth and topographical changes in plate structures using sideband peak count-index and topological acoustic sensing techniques. *Ultrasonics* **2024**, *141*, 107354. [CrossRef] [PubMed]

Sensors **2024**, 24, 6552 17 of 17

32. Zhang, G.; Li, X.; Kundu, T. Ordinary state-based peri-ultrasound modeling to study the effects of multiple cracks on the nonlinear response of plate structures. *Ultrasonics* **2023**, *133*, 107028. [CrossRef] [PubMed]

- 33. Zhang, G.; Li, X.; Zhang, S.; Kundu, T. Sideband peak count-index technique for monitoring multiple cracks in plate structures using ordinary state-based peri-ultrasound theory. *J. Acoust. Soc. Am.* **2022**, *152*, 3035–3048. [CrossRef] [PubMed]
- 34. Zhang, G.; Li, X.; Li, T.; Kundu, T. Ordinary state-based peri-ultrasound modeling for monitoring crack propagation in plate structures using sideband peak count-index technique. *J. Sound Vib.* **2024**, *568*, 117962. [CrossRef]
- Jhang, K.-Y. Nonlinear ultrasonic techniques for nondestructive assessment of micro damage in material: A review. Int. J. Precis. Eng. Manuf. 2009, 10, 123–135, Erratum in Int. J. Precis. Eng. Manuf. 2017, 18, 139. [CrossRef]
- 36. Kawashima, K.; Omote, R.; Ito, T.; Fujita, H.; Shima, T. Nonlinear acoustic response through minute surface cracks: FEM simulation and ex-perimentation. *Ultrasonics* **2002**, *40*, 611–615. [CrossRef]
- 37. Kim, Y.; Choi, S.; Jhang, K.-Y.; Kim, T. Experimental Verification of Contact Acoustic Nonlinearity at Rough Contact Interfaces. *Materials* **2021**, *14*, 2988. [CrossRef]
- 38. He, Y.; Xiao, Y.; Su, Z.; Pan, Y.; Zhang, Z. Contact acoustic nonlinearity effect on the vibro-acoustic modulation of delaminated composite structures. *Mech. Syst. Signal Process.* **2022**, *163*, 108161. [CrossRef]
- 39. Zhang, G.; Li, X.; Kundu, T. Peri-Ultrasound Modeling to Investigate the Performance of Different Nonlinear Ultrasonic Techniques for Damage Monitoring in Plate Structures. *J. Nondestruct. Eval. Diagn. Progn. Eng. Syst.* **2024**, *7*, 031003. [CrossRef]
- 40. Guan, L.; Zou, M.; Wan, X.; Li, Y. Nonlinear Lamb Wave Micro-Crack Direction Identification in Plates with Mixed-Frequency Technique. *Appl. Sci.* **2020**, *10*, 2135. [CrossRef]
- 41. Castellano, A.; Fraddosio, A.; Piccioni, M.D.; Kundu, T. Linear and Nonlinear Ultrasonic Techniques for Monitoring Stress-Induced Damages in Concrete. *J. Nondestruct. Eval. Diagn. Progn. Eng. Syst.* **2021**, *4*, 041001. [CrossRef]
- 42. Alnuaimi, H.N.; Amjad, U.; Russo, P.; Lopresto, V.; Kundu, T. Advanced non-linear ultrasonic sideband peak count-index technique for efficient detection and monitoring of defects in composite plates. *J. Vib. Control.* 2023, 10775463231168228. [CrossRef]
- 43. Ho, I.-T.; Muralidharan, K.; Runge, K.; Granados, A.H.; Kundu, T.; Deymier, P.A. Monitoring defects in plates using topological acoustic sensing and sideband peak counting. *Ultrasonics*, 2024; Under review.

**Disclaimer/Publisher's Note:** The statements, opinions and data contained in all publications are solely those of the individual author(s) and contributor(s) and not of MDPI and/or the editor(s). MDPI and/or the editor(s) disclaim responsibility for any injury to people or property resulting from any ideas, methods, instructions or products referred to in the content.